Outage Probability Analysis of Uplink Heterogeneous Non-terrestrial Networks: A Novel Stochastic Geometry Model

Wen-Yu Dong, Shaoshi Yang, *Senior Member, IEEE*, Wei Lin, Wei Zhao, Jia-Xing Gui, and Sheng Chen, *Life Fellow, IEEE*

***Abstract*—In harsh environments such as mountainous terrain, dense vegetation areas, or urban landscapes, a single type of unmanned aerial vehicles (UAVs) may encounter challenges like flight restrictions, difficulty in task execution, or increased risk. Therefore, employing multiple types of UAVs, along with satellite assistance, to collaborate becomes essential in such scenarios. In this context, we present a stochastic geometry based approach for modeling the heterogeneous non-terrestrial networks (NTNs) by using the classical binomial point process and introducing a novel point process, called Matérn hard-core cluster process (MHCCP). Our MHCCP possesses both the exclusivity and the clustering properties, thus it can better model the aircraft group composed of multiple clusters. Then, we derive closed-form expressions of the outage probability (OP) for the uplink (aerial-to-satellite) of heterogeneous NTNs. Unlike existing studies, our analysis relies on a more advanced system configuration, where the integration of beamforming and frequency division multiple access, and the shadowed-Rician (SR) fading model for interference power, are considered. The accuracy of our theoretical derivation is confirmed by Monte Carlo simulations. Our research offers fundamental insights into the system-level performance optimization of NTNs.**

***Index Terms*—Heterogeneous non-terrestrial networks, stochastic geometry, Matérn hard-core cluster process, binomial point process, outage probability.**

I. Introduction

Non-terrestrial networks (NTNs), encompassing unmanned aerial vehicles (UAVs), high-altitude platforms (HAPs), and satellite networks, are commonly utilized for a variety of purposes such as remote sensing, navigation, disaster management, and other commercial applications [1]. However, in specific environments, singular-type low-altitude UAVs may confront challenges such as flight restrictions, task execution difficulties, or heightened risks. For instance, in rugged terrains like mountainous regions, densely vegetated areas, or urban landscapes, one UAV type may outperform others, necessitating the integration of multiple low-altitude UAV types in a heterogeneous configuration. Therefore, employing multiple types of low-altitude UAVs in a heterogeneous configuration is crucial.

However, in challenging terrains, substantial shadow fading occurs due to obstructions like buildings, trees, and mountains, rendering conventional fading models such as Rayleigh, Rician, and Nakagami less applicable. In heterogeneous non-ground networks, the presence of multiple types of UAVs, their spatial distribution, and communication characteristics all contribute to the complexity of analysis. Therefore, conventional research methods often rely on discrete event simulations or network simulators, which lack the use of mathematical methods [2, 3] to comprehensively study the potential features of networks. Additionally, these methods tend to impose notable constraints when applied to specific network contexts. Recent studies have demonstrated that stochastic geometry [4] and random geometric graphs [5] have emerged as highly effective tools for addressing the aforementioned challenges.

In contrast to Rayleigh and Nakagami-m fading, shadowed-Rician (SR) fading [6] has been proven to be more appropriate for the statistical characterization of satellite channels. This model has been found to be applicable across several frequency bands, such as S-, L-, Ku-, and Ka-band, making it a versatile choice for modeling satellite communication channels. While the SR model is extensively employed in satellite link research, system-level analysis is understudied. With LEO satellites located at different altitudes, the work [7] investigated the joint coverage probability from satellites to satellite gateways in remote areas and then to anchor base stations, given that the satellite-to-gateway link is subject to SR fading. The authors of [8] derived the downlink OP of the LEO satellite communication system under SR fading based on a BPP distribution and optimized the system throughput under visibility and outage constraints. Nevertheless, similar to majority of the works utilizing SR models, these two papers solely examined SNR while neglecting the consideration of interference. The works [9] and [10] approximated the squared SR model with a Gamma random variable and solves the interruption probability using a Gamma function model. Song *et al.* [11] employed the Nakagami-m fading model rather than the SR fading model for the purpose of estimating statistical values of interference. Hence, it is evident that the interference analysis with the SR model remains unexplored.

Motivated by the aforementioned discoveries, this study investigates the heterogeneous NTN system, comprising two distinct groups of airplanes and one satellite. To better model such a heterogeneous NTN, we introduce a novel point model called Matérn hard-core cluster process (MHCCP), which is derived by combining or integrating type-II Matérn hard-core point process (MHCPP) and Matérn cluster process (MCP). The location distributions of these two aircraft groups are described as the MHCCP for one group and the BPP for the other group. Furthermore, beamforming and frequency

W.-Y. Dong, S. Yang, W. Lin, W. Zhao, and J.-X Gui are with the School of Information and Communication Engineering, Beijing University of Posts and Telecommunications, with the Key Laboratory of Universal Wireless Communications, Ministry of Education, and also with the State Key Laboratory of Networking and Switching Technology, Beijing 100876, China (E-mails: wenyu.dong@bupt.edu.cn, shaoshi.yang@bupt.edu.cn, linwei@bupt.edu.cn, wei.zhao@bupt.edu.cn, jiaxing.gui@bupt.edu.cn).

S. Chen is with the School of Electronics and Computer Science, University of Southampton, Southampton SO17 1BJ, U.K. (E-mail: sqc@ecs.soton.ac.uk).

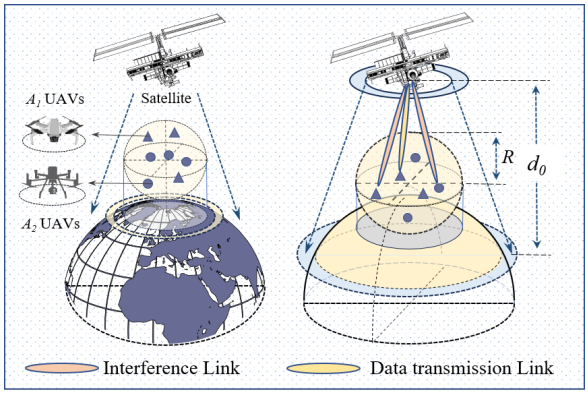

Fig. 1. Illustration of the heterogeneous NTN system.

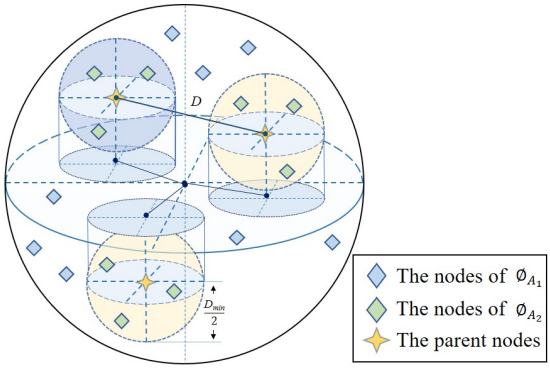

Fig. 2. Illustration of node positions in heterogeneous aircraft network.

division multiple access (FDMA) are employed to improve network efficiency. Since in this heterogeneous NTN system, nodes operating within the same subchannel share the same frequency band, we explicitly investigate the effects of multi-user interference (MUI) under SR fading channels. Our contributions can be succinctly summarized through the following four key points.

- Unlike existing studies, we consider a more advanced and comprehensive system model, which involves many factors, such as network deployment, multi-access mechanisms, beam models, and channel models, when analyzing the performance of heterogeneous NTNs.
- Different from what is often overlooked in previous research work, we consider interference in the presence of SR fading, while conducting the uplink performance analysis for heterogeneous satellite-aerial networks (SANs).
- Compared to other similar articles, we introduce a novel point process model, referred to as the MHCCP, that offers a comprehensive representation of both the clustering and exclusion properties of nodes.
- We verify through Monte Carlo simulation that our analysis of uplink performance for heterogeneous SANs is highly accurate, and discuss the impact of different parameters.

The remainder of this paper is organized as follows: In Section II, the system model is presented. Section III provides our primary performance analysis results. In Section IV, we provide numerical results to verify our theoretical derivations and to study the effect of key system parameters. Finally, our conclusions are drawn in Section V.

II. System Model

We consider a SAN composed of a satellite (LEO satellite S) as well as two heterogeneous UAV groups (A_1 and A_2), as shown in Fig. 1. The two groups of heterogeneous UAVs exhibit distinct features in terms of their parameters and transmitter capacity. For instance, in tasks like geological disaster detection, UAV group A_1 operate in clustered formations to survey surface areas, while UAV A_2 functions individually, offering flexibility to explore challenging terrains such as canyons, mountainous regions, and indoor structures for localized monitoring and reconnaissance. Considering that UAV coverage areas are much smaller than the distances to satellites, we opt to model both A_1 and A_2 within the same spherical space. This approach simplifies the description without affecting the derived results, even when two heterogeneous UAV swarms are not situated in the same spherical space. The trajectories of satellites can be predicted and the wide angle of their receiver antenna is large. Our analysis focuses on the uplink connection between UAV groups and a specific satellite.

A. Topology Model

1) Deployment of A_1 and A_2: According to [12], it is impossible to accurately describe networks with a finite number of nodes and limited area using the PPP. In practical applications, A_1 typically consists of a finite number of nodes and operates within a limited-size region. Therefore, we posit that A_1 adheres to the principle of the BPP ϕ_{A_1}, with a numerical value of N_1, within the spherical region $\mathcal{V}$ of radius R. Furthermore, the MHCCP is utilized in order to represent the clustered networking of A_2, which allows for the maintenance of a secure distance between different clusters within A_2, facilitating cooperative operations. Fig. 2 illustrates the distribution of node locations for A_1 and A_2.

Next, we outline the three-step approach involved in the construction of MHCCP, denoted as ϕ_{A_2}.

In the first step, candidate points are generated in a uniform manner using a homogeneous PPP with the density λ_1, within the spherical space $\mathcal{V}$. The radius of $\mathcal{V}$ is R_1, and the volume of $\mathcal{V}$ is V_1. In relation to the number of candidate points, denoted as N_c, the probability mass function of the Poisson distribution can be represented as $\mathbb{P}(N_c = s) = \frac{\lambda_1 V_1}{s!}\exp(-\lambda_1 V_1)$, where s is the number of the candidate points.

In the second step, each candidate point is assigned with an independent mark, randomly selected from a uniform distribution within the range $[0,\ 1]$. Subsequently, we exclusively retain the point with the smallest mark within a confined spherical space with the radius $D_{\min}$ by eliminating the others. Specifically, for a specific point Q serving as the center of a small spherical repulsion space with the radius $D_{\min}$, if there are other candidate points within this spherical repulsion space, their mark values are compared, and only the point with

the smallest mark is preserved within each spherical repulsion space. This process iterates for each candidate point until each spherical repulsion space contains only one point. After this removal process, the distance D between any two points is larger than or equal to $D_{\min}$, and we have constructed the MHCPP, denoted as ϕ_c, with the density λ_2 which can be expressed mathematically as $\lambda_2 = \frac{1-\exp(-\frac{4}{3}\pi D_{\min}^3 \lambda_1)}{\frac{4}{3}\pi D_{\min}^3}$.

In the final step, we exploit the principle of MCP by considering the points in ϕ_c as the parent points, and uniformly generate subpoints within the sphere of radius $D_{\min}/2$ around each parent point. The number of subpoints in each cluster follows a Poisson distribution with parameter $\bar{c}$. Through this clustering process, we complete the MHCCP construction, and all the subpoints generated form ϕ_{A_2}. The relationship between the density of the parent points, λ_2, and the density of ϕ_{A_2}, λ_3, is expressed by $\lambda_3 = \lambda_2 \bar{c}$.

2) Multi-access Mechanism: Multi-access mechanisms in aerial-to-satellite communications play an important role in improving the uplink transmission performance. To enhance the network's connectivity and capacity, the FDMA is employed, implementing frequency reuse across a total of K orthogonal frequency channels ($K \leq N_1$). To enable communication with the satellite on a cluster basis, the number of frequency bands in A2 is an integer multiple of the clusters, i.e., N_2/K is expected to be an integer which is multiple of $\bar{c}$. For the purpose of simplifying calculations, we assume that $N_1/K + N_2/K$ aerial transmitters share a common frequency channel, thereby causing co-channel interference. Hence, we randomly select one channel from the $(N_1+N_2)/K$ available channels for investigation, and denote the sets of nodes from the two UAV groups sharing the same frequency band as ϕ_1 and ϕ_2, respectively.

B. Channel Model

1) Directional Beamforming Modeling: To enhance the strength of the received signal and optimize transmission performance, directional beamforming is employed at aerial transmitters and satellite receivers. To simplify processing, the actual antenna is approximated using a sector antenna model. Due to the extensive coverage capability of the satellite, it is reasonable to assume that the satellite receiver can effectively capture the signals transmitted by the UAVs through the primary lobe. The overall directional gain of link l is denoted as D_l, and θ represents the angular breadth of the primary lobe of transmitter. In this context, G_t and g_t refer to the transmitter array gains of the main and side lobes, respectively. Similarly, G_r denotes the receiver array main lobe gain.

The value of D_m for the link from a given target node m to the satellite receiver is equal to the product of G_t and G_r, i.e., $D_m = G_t G_r$. On the other hand, the value of D_{x_l} for any other interference node x_l is determined by the directivity gains of the main and side lobes of the antenna beam pattern. Accordingly, we have the probability distribution model expression of D_{x_l} as:

$$D_{x_l} = \begin{cases} G_t G_r, & \mathrm{P}_{M,M} = \frac{\theta}{2\pi}, \\ g_t G_r, & \mathrm{P}_{S,M} = 1 - \frac{\theta}{2\pi}, \end{cases} \tag{1}$$

where the indices M and S denote the main and side lobes, respectively, and $\mathrm{P}_{t,M}$, $t \in \{M, S\}$, denotes the probability of the link in state $\{t, M\}$.

2) Channel Fading: In this paper, the presence of abundant shadows due to complex terrain, along with the predominant propagation path being the Line-of-Sight (LoS) path, closely aligns with the characteristics of SR fading. Therefore, utilizing SR fading for modeling the aerial-satellite link in complex terrain at low altitudes is reasonable. We define $2c$ as the mean power of the multi-path component excluding the LoS component, Ω as the average power of the LoS component, and q as the Nakagami-m fading parameter. The small-scale fading is represented as $|h|^2$ in this study. The probability density function (PDF) of $|h|^2$ can be mathematically stated as [13]

$$f_{|h|^2}(x) = \kappa \, \exp(-\beta x) \, {}_1F_1(q; 1; \delta x), \tag{2}$$

where $\kappa = \frac{(2cq)^q}{2c(2cq+\Omega)^q}$, $\delta = \frac{\Omega}{2c(2cq+\Omega)}$, $\beta = \frac{1}{2c}$ and ${}_1F_1(\cdot;\cdot;\cdot)$ is the confluent hypergeometric function of the first kind..

C. SINR Model

In accordance with the aforementioned model, the SINR, a critical metric for evaluating wireless link performance, can be expressed as:

$$\mathrm{SINR} = \frac{p_m D_m |h_m|^2 d_m^{-\alpha}}{I + \sigma^2}, \tag{3}$$

where $I = \sum_{l\in\{1,2\}} \sum_{x_l \in \phi_l \setminus \{m\}} p_{x_l} D_{x_l} |h_{x_l}|^2 d_{x_l}^{-\alpha}$, l is the index of a particular UAV gruop in A_1 and A_2, m and x_l are the target node and interference nodes, p_m and p_{x_l} are the transmit power at m and x_l, while d_m is the distance between m and the satellite, d_{x_l} is the distance between x_l and the satellite, α is the path-loss exponent, and σ^2 is the strength of additive white Gaussian noise (AWGN).

III. Performances Analysis

This section analyzes the OP for the proposed heterogeneous SAN model. Without loss of generality, we assume uniform transmission power level for all transmitters within each aircraft group, except for the target transmitter. Specifically, except for the target transmitter m whose power is set to p_m, the power levels for aircraft in the two groups, ϕ_{A_1} and ϕ_{A_2}, are given by p_1 and p_2, respectively.

The OP refers to the likelihood that the SINR at the receiver is insufficient to meet the minimum SINR required for successful data transmission. Thus, the OP of the aerial-to-satellite link is defined by

$$P_{\mathrm{out}} \triangleq \mathbb{P}(\mathrm{SINR} \leq T) = \mathbb{P}\left(\frac{p_m D_m |h_m|^2 d_m^{-\alpha}}{I + \sigma^2} \leq T\right), \tag{4}$$

where T is the SINR threshold. The following theorem derives a useful expression for OP.

Theorem 1. *The outage probability for an arbitrarily located aerial node under the SR fading channel is given by*

$$\begin{aligned}P_{\text{out}} &\triangleq \mathbb{P}(\text{SINR} \leq T)\\ &= \sum_{k=0}^{\infty} \frac{\Psi(k)}{(\beta-\delta)^{k+1}}\Gamma(k+1)\sum_{t=0}^{k+1}\binom{k+1}{t}(-1)^t\\ &\quad\times \mathbb{E}\left[\exp\left(-s(I+\sigma^2)\right)\right], \end{aligned} \tag{5}$$

where $\Psi(k) = \frac{(-1)^k\kappa\delta^k}{(k!)^2}\text{Ps}(1-q)_k$, $s = \frac{t\zeta(\beta-\delta)Td_m^{\alpha}}{p_m D_m}$ *and* $\zeta = \left(\Gamma(k+2)\right)^{-\frac{1}{k+1}}$.

Proof. Using the Kummer's transform of the hypergeometric function, we can rewrite the PDF of $|h|^2$ as $f_{|h|^2}(x) = \sum_{k=0}^{\infty}\Psi(k)x^k\exp(-(\beta-\delta)x$, where $\Psi(k) = \frac{(-1)^k\kappa\delta^k}{(k!)^2}\text{Ps}(1-q)_k$ and the Pochhammer symbol is defined as $\text{Ps}(x)_n = \Gamma(x+n)/\Gamma(x)$. Then, the CDF of $|h|^2$ can be represented as

$$\begin{aligned}F_{|h|^2}(x) &= \sum_{k=0}^{\infty}\Psi(k)\int_0^x t^k\exp(-(\beta-\delta)t)\text{d}t\\ &= \sum_{k=0}^{\infty}\frac{\Psi(k)}{(\beta-\delta)^{k+1}}\gamma(k+1,(\beta-\delta)x). \end{aligned} \tag{6}$$

Therefore, we can obtain P_{out} as

$$\begin{aligned}P_{\text{out}} &\triangleq \mathbb{P}\left(\frac{p_m D_m|h_m|^2 d_m^{-\alpha}}{I+\sigma^2} \leq T\right)\\ &= \mathbb{E}\left[\kappa\sum_{k=0}^{\infty}\frac{\Psi(k)}{(\beta-\delta)^{k+1}}\gamma\left(k+1,(\beta-\delta)\frac{T(I+\sigma^2)d_m^{\alpha}}{p_m D_m}\right)\right]\\ &\overset{(a)}{\approx} \mathbb{E}\Bigg[\sum_{k=0}^{\infty}\frac{\Psi(k)}{(\beta-\delta)^{k+1}}\Gamma(k+1)\\ &\quad\times\left(1-\exp\left(-\frac{\zeta(\beta-\delta)T(I+\sigma^2)d_m^{\alpha}}{p_m D_m}\right)\right)^{k+1}\Bigg]\\ &\overset{(b)}{=} \sum_{k=0}^{\infty}\frac{\Psi(k)}{(\beta-\delta)^{k+1}}\Gamma(k+1)\sum_{t=0}^{k+1}\binom{k+1}{t}(-1)^t\\ &\quad\times\mathbb{E}\left[\exp(-s(I+\sigma^2))\right], \end{aligned} \tag{7}$$

where (a) is approximated by using $\gamma(k+1,x) < \Gamma(k+1)(1-\exp(-\zeta x))^{k+1}$ [14], $\zeta = \left(\Gamma(k+2)\right)^{-\frac{1}{k+1}}$, and (b) is obtained from the binomial theorem with $s = \frac{t\zeta(\beta-\delta)Td_m^{\alpha}}{p_m D_m}$. This completes the proof. □

Given that the distances between aerial nodes in finite-area networks are typically limited to a few kilometers, while the distance to the satellite extends to the range of hundreds or even thousands of kilometers, it is reasonable to assert that the latter is significantly greater in magnitude than the former. Therefore, it is assumed that all the aerial transmitters possess an equal transmission distance to the satellite, i.e., $d_m = d_{x_l} = d_0$. Subsequently, we obtain

$$\mathbb{E}\left[\exp(-s(I+\sigma^2))\right] = \exp(-s\sigma^2)\mathcal{L}_I(s), \tag{8}$$

where $\mathcal{L}_I(s)$ is the Laplace transform of the cumulative interference power I that is expressed in Lemma 1.

Lemma 1. *The Laplace transform of random variable I is:*

$$\begin{aligned}\mathcal{L}_I(s) &= \mathbb{E}[\exp(-sI)]\\ &= (M_2(1))^{n_1}\exp\left(\lambda_3 V_1(M_2(2)-1)\right), \end{aligned} \tag{9}$$

where $V_1 = \frac{4\pi R_1^3}{3}$, $\lambda_3 = \bar{c}\,\frac{1-\exp\left(-\frac{4}{3}\pi D_{\min}^3\lambda_1\right)}{\frac{4}{3}\pi D_{\min}^3}$, $M_2(l) = M_1(\mu_l)\frac{\theta}{2\pi} + M_1(\nu_l)(1-\frac{\theta}{2\pi})$, $l \in \{1,2\}$, *with* $M_1(t_l) = \frac{(2cq)^q(1+2ct_l)^{q-1}}{\left((2cq+\Omega)(1+2ct_l)-\Omega\right)^q}$, $t_l \in \{\mu_l,\nu_l\}$, $\mu_l = -sp_l d_0^{-\alpha}G_t G_r$ *and* $\nu_l = -sp_l d_0^{-\alpha}g_t G_r$, *and when the target UAV node is in* ϕ_1 *and* ϕ_2, n_1 *is given by* $\frac{N_1}{K}-1$ *and* $\frac{N_1}{K}$, *respectively.*

Proof.

$$\begin{aligned}\mathcal{L}_I(s) &= \mathbb{E}\left[\exp(-sI)\right]\\ &= \mathbb{E}\left[\exp\left(-s\sum_{l\in\{1,2\}}\sum_{x_l\in\phi_l\setminus\{m\}}p_l D_{x_l}|h_{x_l}|^2 d_{x_l}^{-\alpha}\right)\right]. \end{aligned} \tag{10}$$

As the point process and the fading process are independent of each other, $\mathcal{L}_I(s)$ can be expressed as

$$\begin{aligned}\mathcal{L}_I(s) &= \mathbb{E}\left[\prod_{l\in\{1,2\}}\prod_{x_l\in\phi_l\setminus\{m\}}\mathbb{E}_{|h_{x_l}|^2}\left[\exp\left(-sp_l D_{x_l}|h_{x_l}|^2 d_{x_l}^{-\alpha}\right)\right]\right]\\ &\overset{(a)}{=} \mathbb{E}_{N_l}\left[\prod_{l\in\{1,2\}}\prod_{x_l\in\phi_l\setminus\{m\}}\mathbb{E}_{D_{x_l},|h_{x_l}|^2}\left[\exp\left(-t_l|h_{x_l}|^2\right)\right]\right], \end{aligned} \tag{11}$$

where (a) is obtained by assuming that all the aerial transmitters have the same transmission distance and denoting $t_l = sp_l D_{x_l} d_0^{-\alpha}$.

As shown in [15], the moment-generating function of the SR model is defined as $M_S(x) = \mathbb{E}\left[\exp(-xS)\right] = \frac{(2cq)^q(1+2cx)^{q-1}}{((2cq+\Omega)(1+2cx)-\Omega)^q}$. Thus, we further obtain

$$\begin{aligned}\mathcal{L}_I(s) &= \mathbb{E}_{N_l}\Bigg[\prod_{l\in\{1,2\}}\prod_{x_l\in\phi_l\setminus\{m\}}\mathbb{E}_{D_{x_l}}\underbrace{\left[\frac{(2cq)^q(1+2ct_l)^{q-1}}{((2cq+\Omega)(1+2ct_l)-\Omega)^q}\right]}_{M_1(t_l)}\Bigg]\\ &\overset{(b)}{=} \mathbb{E}_{N_l}\Bigg[\prod_{l\in\{1,2\}}\prod_{x_l\in\phi_l\setminus\{m\}}\underbrace{\left[M_1(\mu_l)\frac{\theta}{2\pi}+M_1(\nu_l)\left(1-\frac{\theta}{2\pi}\right)\right]}_{M_2(l)}\Bigg]\\ &= \mathbb{E}_{N_1}\Bigg[\prod_{x_1\in\phi_1\setminus\{m\}}M_2(1)\Bigg]\mathbb{E}_{N_2}\Bigg[\prod_{x_2\in\phi_2\setminus\{m\}}M_2(2)\Bigg]\\ &\overset{(c)}{=} \sum_{n=1}^{n_1}\binom{n_1}{n}P_I^n(1-P_I)^{n_1-n}\left(M_2(1)\right)^n\\ &\quad\times\sum_{n_2=0}^{\infty}\frac{(\lambda_3 V_1)^{n_2}}{n_2!}\exp(-\lambda_3 V_1)(M_2(2))^{n_2}\\ &\overset{(d)}{=} (M_2(1))^{n_1}\exp\left(\lambda_3 V_1(M_2(2)-1)\right), \end{aligned} \tag{12}$$

where (b) is obtained by denoting $\mu_l = sp_l d_0^{-\alpha}G_t G_r$ and $\nu_l = sp_l d_0^{-\alpha}g_t G_r$, (c) is obtained by the fact that ϕ_{A_1} follows

the BPP with P_I being the proportion of the interfering nodes to the total number of nodes in ϕ_{A_1}, ϕ_{A_2} follows the PPP with the density of λ_3 and the volume of the spherical space $\mathcal{V}$ is $V_1 = \frac{4\pi R_1^3}{3}$, and (d) is obtained by the fact that all the nodes in ϕ_{A_1} are interference nodes and hence $P_I = 1$. This completes the proof. □

Remark 1. *The MHCCP model exhibits strong repulsion between clusters, which is determined by the minimum distance separating them. Consequently, the system's total number of nodes cannot exhibit unlimited growth as λ_1 rises. In order to ascertain the upper limit of nodes in this system, we differentiate the function λ_3 over λ_1, yielding $\frac{\mathrm{d}\lambda_3}{\mathrm{d}\lambda_1} = \overline{c}\left(\frac{4}{3}\pi D_{\min}^3\right)^2 \exp\left(-\frac{4}{3}\pi D_{\min}^3 \lambda_1\right)$. Notably, $\frac{\mathrm{d}\lambda_3}{\mathrm{d}\lambda_1} \geq 0$. Moreover, $\lim_{\lambda_1 \to \infty} \frac{\mathrm{d}\lambda_3}{\mathrm{d}\lambda_1} = 0$. Hence, the upper limit of λ_3 can be established as $\lim_{\lambda_1 \to \infty} \lambda_3 = \frac{3\overline{c}}{4\pi D_{\min}^3}$, whose validity will be further examined in the simulation discussed in Section IV.*

By substituting (8) and (9) into (5) and noting the definitions of Lemma 1, we can obtain the analytical closed-form expression for the OP.

IV. Numerical Results

In this section, we validate the derived theoretical expressions by Monte-Carlo simulations with a total of 50,000 iterations. Unless otherwise explicitly specified, the default simulation system parameters detailed in Table I are used. The outcomes obtained from the analytical expressions derived in Section III are labeled as 'Analysis', whilst the Monte Carlo findings are labeled as 'Simulation'.

TABLE I
Default Parameter of Simulation System.

Notation	Parameter	Values
d_0	Distance between UAVs and satellite	300km
R_1	Radius of $\mathcal{V}$	10km
$D_{\min}$	Minimum distance of candidate pairs	1km
p_1, p_2	Power of transmitters in A_1 and A_2	20dBW, 19dBW
λ_1	Density of candidate points	10^{-11}
$\mathcal{SR}(c, q, \Omega)$	SR fading model	$\mathcal{SR}(0.158, 1, 0.1)$
α	Path-loss exponent	2
T	SINR threshold	-18dB
σ^2	AWGN's power spectral density	-160dBm/Hz

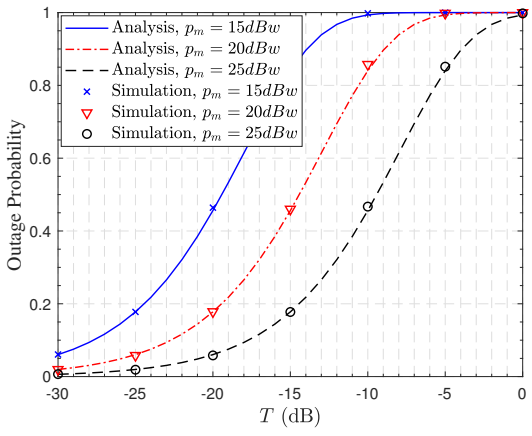

Fig. 3. Outage probability as function of SINR threshold T, given different transmit power p_m of target node.

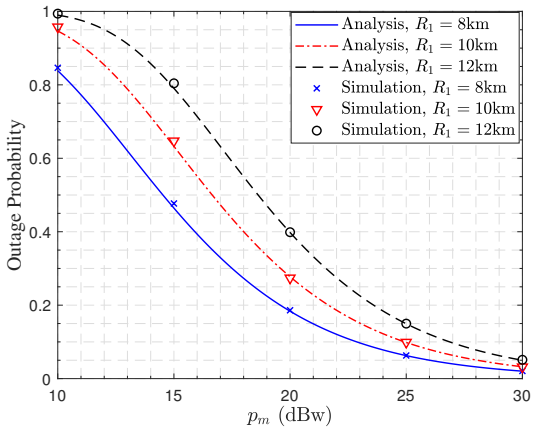

Fig. 4. Outage probability as function of target node transmit power p_m, given different values of spherical space's radius R_1.

These simulations are utilized to generate the plots depicting the simulated OP performance of the heterogeneous aerial-to-satellite uplink. We observe that the analytical results exhibit a high degree of concordance with the corresponding simulation results, hence bolstering the credibility and soundness of our theoretical investigation presented in Section III.

First Fig. 3 depicts the OP as the function of the SINR threshold T, given three different values of the target node's transmit power p_m. It can be seen from Fig. 3 that as the SINR threshold T increases, the OP also increases. This is due to the inverse relationship between T and the possibility of achieving a SINR that surpasses the given threshold value. Hence, once the threshold value reaches to a specific level, the likelihood of disruption occurring in the link between the aerial transmitter and the satellite reaches its maximum value of 1. Furthermore, increasing the power of the target transmitter leads to an increase in its SINR and this reduces the risk of communication interruption. Therefore, with an increase in p_m, the OP curve exhibits a rightward shift.

Next Fig. 4 plots the OP as the function of p_m, given three different values for the radius R_1 of the spherical space $\mathcal{V}$. As expected, increasing p_m decreases the OP. Also it can be seen that the expansion of the distribution space of aerial

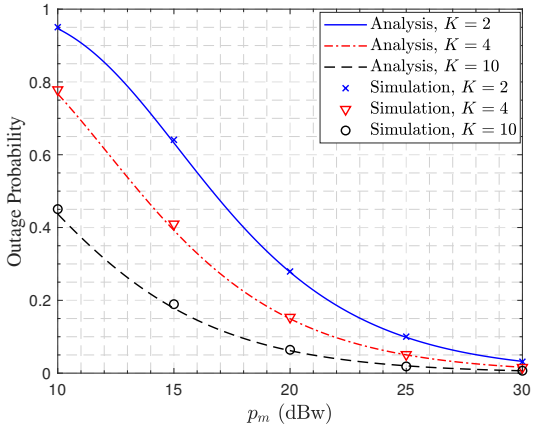

Fig. 5. Outage probability as function of target node transmit power p_m, given different numbers of frequency channels K.

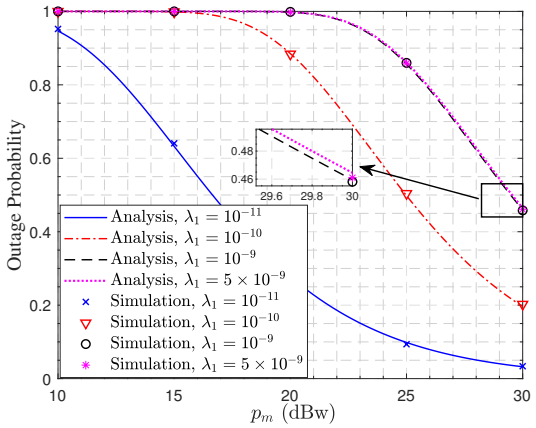

Fig. 6. Outage probability as function of target node transmit power p_m, given different numbers of frequency channels K.

transmitters leads to a noticeably worse OP performance. This is because the increased availability of space for the MHCCP deployment of air nodes results in a higher number of transmitters concurrently attempting to access the satellite, leading to a higher MUI and consequently a worsen OP performance.

Then fig. 5 provides a clear visual representation of the influence of the number of frequency channels K on the OP, indicating that increasing K decreases the OP. Evidently, providing more frequency channels enables more transmitters operate in orthogonal access mode, thereby resulting in a reduction of the interference towards the intended transmitter. Consequently, the SINR of the target link increases, diminishing the likelihood of interruption.

Fig. 6 depicts the OP as the function of p_m, given four different values for the density of candidate points λ_1. As expected, increasing λ_1 increases number of nodes, which results in greater MUI and consequently increases the OP. However, as can be seen from Fig. 6, when λ_1 increases beyond 10^{-9}, the OP appears saturated. This is because the imposed minimum spacing $D_{\min}$ prevents the number of nodes from infinitely escalating as the density increases.

V. Conclusions

In this paper, we have proposed a tractable approach for analyzing the outage probability for the uplink of heterogeneous satellite-aerial networks. Our proposed novel point model can better describe the clustering distribution of aircraft Our novel contribution has been two-fold. Then, the interference analysis template we provide for the SR model is applicable to many other related derivation studies. Finally, the exact closed form solution expression for the interruption probability we derived can be directly applied in similar scenarios, thereby quickly obtaining performance analysis of the network. Our study therefore offers theoretical guidance and valuable insights for the actual deployment of heterogeneous satellite-aerial networks.

References

[1] M. M. Azari *et al.*, "Evolution of non-terrestrial networks from 5G to 6G: A survey," *IEEE Commun. Surveys & Tuts.*, vol. 24, no. 4, pp. 2633–2672, 4th Quart. 2022.

[2] J. Y. Chen, "UAV-guided navigation for ground robot teleoperation in a military reconnaissance environment," *Ergonomics*, vol. 53, no. 8, pp. 940–950, Jul. 2010.

[3] M. A. Ma'Sum *et al.*, "Simulation of intelligent Unmanned Aerial Vehicle (UAV) for military surveillance," in *Proc. Int. Conf. Advanced Computer Science and Information Syst. (ICACSIS)*, Sep. 2013, pp. 161–166.

[4] W. K. D. Stoyan and J. Mecke, *Stochastic geometry and its applications*. John Wiley & Sons, 1996.

[5] J. Dall and M. Christensen, "Random geometric graphs," *Phys. Rev. E*, vol. 66, no. 1, pp. 16 121–16 121, Jul. 2002.

[6] C. Loo, "A statistical model for a land mobile satellite link," *IEEE Trans. Veh. Technol.*, vol. 34, no. 3, pp. 122–127, Aug. 1985.

[7] A. Talgat, M. A. Kishk, and M. S. Alouini, "Stochastic geometry-based analysis of LEO satellite communication systems," *IEEE Commun. Lett.*, no. 8, p. 25, Aug. 2021.

[8] D.-H. Jung, J.-G. Ryu, W.-J. Byun, and J. Choi, "Performance analysis of satellite communication system under the shadowed-Rician fading: A stochastic geometry approach," *IEEE Trans. Commun.*, vol. 70, no. 4, pp. 2707–2721, Apr. 2022.

[9] M. Sellathurai, S. Vuppala, and T. Ratnarajah, "User selection for multi-beam satellite channels: A stochastic geometry perspective," in *Proc. 50th Asilomar Conf. Signals, Syst. Comput.*, Nov. 2016, pp. 487–491.

[10] O. Y. Kolawole, S. Vuppala, M. Sellathurai, and T. Ratnarajah, "On the performance of cognitive satellite-terrestrial networks," *IEEE Trans. Cogn. Commun. Netw*, vol. 3, no. 4, pp. 668–683, Dec. 2017.

[11] Z. Song *et al.*, "Cooperative satellite-aerial-terrestrial systems: A stochastic geometry model," *IEEE Trans. Wireless Commun.*, vol. 22, no. 1, pp. 220–236, Jan. 2023.

[12] S. Srinivasa and M. Haenggi, "Distance distributions in finite uniformly random networks: Theory and applications," *IEEE Trans. Veh. Technol.*, vol. 59, no. 2, pp. 940–949, Feb. 2010.

[13] X. Zhang, D. Guo, K. An, Z. Chen, B. Zhao, Y. Ni, and B. Zhang, "Performance analysis of NOMA-based cooperative spectrum sharing in hybrid satellite-terrestrial networks," *IEEE Access*, vol. 7, pp. 172 321–172 329, Nov. 2019.

[14] H. Alzer, "On some inequalities for the incomplete gamma function," *Math. Comput.*, vol. 66, no. 218, pp. 771–778, 1997.

[15] A. Abdi, W. Lau, M.-S. Alouini, and M. Kaveh, "A new simple model for land mobile satellite channels: first- and second-order statistics," *IEEE Trans. Commun.*, vol. 2, no. 3, pp. 519–528, May. 2003.